

ARMY RESEARCH LABORATORY



Nonlinear Joint Fusion and Detection of Mines Using Multisensor Data

by Nasser M. Nasrabadi

ARL-TN-314

May 2008

NOTICES

Disclaimers

The findings in this report are not to be construed as an official Department of the Army position unless so designated by other authorized documents.

Citation of manufacturer's or trade names does not constitute an official endorsement or approval of the use thereof.

Destroy this report when it is no longer needed. Do not return it to the originator.

Army Research Laboratory

Adelphi, MD 20783-1197

ARL-TN-314

May 2008

**Nonlinear Joint Fusion and Detection of Mines Using
Multisensor Data**

Nasser M. Nasrabadi
Sensors and Electron Devices Directorate, ARL

REPORT DOCUMENTATION PAGE			Form Approved OMB No. 0704-0188		
Public reporting burden for this collection of information is estimated to average 1 hour per response, including the time for reviewing instructions, searching existing data sources, gathering and maintaining the data needed, and completing and reviewing the collection information. Send comments regarding this burden estimate or any other aspect of this collection of information, including suggestions for reducing the burden, to Department of Defense, Washington Headquarters Services, Directorate for Information Operations and Reports (0704-0188), 1215 Jefferson Davis Highway, Suite 1204, Arlington, VA 22202-4302. Respondents should be aware that notwithstanding any other provision of law, no person shall be subject to any penalty for failing to comply with a collection of information if it does not display a currently valid OMB control number. PLEASE DO NOT RETURN YOUR FORM TO THE ABOVE ADDRESS.					
1. REPORT DATE (DD-MM-YYYY) May 2008		2. REPORT TYPE Final		3. DATES COVERED (From - To) 1 December 2007	
4. TITLE AND SUBTITLE Nonlinear Joint Fusion and Detection of Mines Using Multisensor Data			5a. CONTRACT NUMBER		
			5b. GRANT NUMBER		
			5c. PROGRAM ELEMENT NUMBER		
6. AUTHOR(S) Nasser M. Nasrabadi			5d. PROJECT NUMBER DRI 2007		
			5e. TASK NUMBER		
			5f. WORK UNIT NUMBER		
7. PERFORMING ORGANIZATION NAME(S) AND ADDRESS(ES) U.S. Army Research Laboratory ATTN: AMSRD-ARL-SE-SE Adelphi, MD 20783-1197			8. PERFORMING ORGANIZATION REPORT NUMBER ARL-TN-314		
9. SPONSORING/MONITORING AGENCY NAME(S) AND ADDRESS(ES)			10. SPONSOR/MONITOR'S ACRONYM(S)		
			11. SPONSOR/MONITOR'S REPORT NUMBER(S)		
12. DISTRIBUTION/AVAILABILITY STATEMENT Approved for public release; distribution unlimited.					
13. SUPPLEMENTARY NOTES					
14. ABSTRACT This report describes a new nonlinear joint fusion and anomaly detection technique for mine detection applications using two different types of sensor data (synthetic aperture radar [SAR] and hyperspectral sensor [HS] data). A well-known anomaly detector called the "RX algorithm" is first extended to perform fusion and detection simultaneously at the pixel level by appropriately concatenating the information from the two sensors. This approach is then extended to its nonlinear version. The nonlinear fusion-detection approach is based on the statistical kernel learning theory which explicitly exploits the higher-order dependencies (nonlinear relationships) between the two types of sensor data through an appropriate kernel. Experimental results for detecting anomalies (mines) in hyperspectral imagery are presented for linear and nonlinear joint fusion and detection for a co-registered SAR and HS imagery. The results show that the nonlinear techniques outperform linear versions.					
15. SUBJECT TERMS sensor fusion, nonlinear anomaly detection, hyperspectral detection, joint fusion and detection, kernel RX					
16. SECURITY CLASSIFICATION OF:			17. LIMITATION OF ABSTRACT	18. NUMBER OF PAGES	19a. NAME OF RESPONSIBLE PERSON
a. REPORT	b. ABSTRACT	c. THIS PAGE			19b. TELEPHONE NUMBER (Include area code)
UNCLASSIFIED	UNCLASSIFIED	UNCLASSIFIED	UL	18	Nasser M. Nasrabadi (301) 394-0806

Contents

List of Figures	iv
1. Objective	1
2. Approach	1
2.1 Joint Fusion and Detection Using SAR and HS at the Pixel Level.....	2
2.2 Nonlinear Joint Fusion and Detection Using SAR and HS at the Pixel Level.....	4
3. Results	5
4. Conclusions	7
Distribution List	8

List of Figures

Figure 1. A sliding dual window: an IWR and an OWR.....	2
Figure 2. (a) HS image, (b) SAR image, (c) RX detected mines for HS, (d) RX detected mines for SAR, (e) kernel RX detected mines for HS, (f) kernel RX detected mines for SAR, (g) joint linear fusion/detection RX results, and (h) joint nonlinear fusion/detection KRX results.....	6
Figure 3. The ROC plots for the conventional RX and kernel RX algorithms.....	7

1. Objective

The recent availability of accurately geo-located, multisensor data (collected as part of the Wide Area Airborne Mine Detection program) has created unprecedented opportunities for the exploration of multisensor, target detection algorithms. Even with this high-fidelity data set, the sensor fusion task still presents many daunting challenges. The objective of this Director's Research Initiative (DRI) investigation is to develop a nonlinear joint fusion and detection technique for mine detection applications using two different types of sensor data—synthetic aperture radar SAR data and hyperspectral sensor (HS) data. A well-known anomaly detector, called the RX algorithm,¹ is extended to perform fusion and detection simultaneously at the pixel level by appropriately concatenating the information from the two sensors. This approach is then extended to its nonlinear version. The nonlinear fusion-detection approach is based on the statistical kernel learning theory which explicitly exploits the higher-order dependencies (nonlinear relationships) between the two types of sensor data through an appropriate kernel.

2. Approach

The main purpose of this DRI project is to nonlinearly fuse the information contents in HS and SAR imagery to effectively detect targets of interests (buried and surface mines). Because of the significant differences in basic physical properties and signal dimensionality between these two sensors, fusion of the raw or processed data from these sensors might mitigate the false alarm rate significantly for anomaly detection purposes. In the previous DRI project (FY05), the main focus was on co-registration of the SAR and HS image data. Individually linear and nonlinear signal detection tools for HS and SAR imagery were developed.² In this DRI report, the nonlinear joint fusion and detection technique is summarized and its detection performance on several mine imageries is reported. The proposed approach is to extend the well-known RX anomaly detector and its nonlinear version (the kernel RX algorithm³) to an integrated multiple-sensor data.

¹ Reed, S.; Yu, X. Adaptive Multiple-Band CFAR Detection of an Optical Pattern With Unknown Spectral Distribution. *IEEE Trans. on Acoustics, Speech Signal Process* **1994**, *38* (10), 1760–1770.

² Ranney, K.; Rosario, D.; Nasrabadi, N. M. *Fusion of Synthetic Aperture Radar and Hyperspectral Imagery*; DRI proposal FY05-SED-35 and the final report FY06; U.S. Army Research Laboratory: Adelphi, MD, December 1996.

³ Kwon, H.; Nasrabadi, N. Kernel Orthogonal Subspace Projection for Hyperspectral Signal Classification. *IEEE Transactions on Geoscience and Remote Sensing* **2005**, *43* (12), 2952–2962.

2.1 Joint Fusion and Detection Using SAR and HS at the Pixel Level

In the proposed approach, detection and fusion is done at the pixel level by concatenating each HS spectral pixel with its corresponding high-resolution SAR pixels and then processing the concatenated data by the RX anomaly detector. This approach jointly exploits the linear correlation or dependencies between the two sensors in order to simultaneously fuse and detect the objects of interest. In Reed and Yu,¹ a spectral anomaly detection algorithm was developed for detecting targets of unknown spectral distribution against a background with unknown spectral covariance. This algorithm is now commonly referred to as the RX anomaly detector, which has been successfully applied to many hyperspectral target detection applications. It is now considered as the benchmark anomaly detection algorithm for multispectral/hyperspectral data. The RX algorithm is a constant false alarm rate (CFAR) adaptive anomaly detector which is derived from the Generalized Likelihood Ratio Test. The RX algorithm is based on exploiting the difference between the spectral signatures of an input pixel with its surrounding neighbors. This distance comparison is very similar to the Mahalanobis distance measure calculated by comparing the corresponding wavelengths (spectral bands) of two measurements. The RX algorithm assumes that the covariance of the background clutter is unknown or calculated from the data. In the conventional RX algorithm, a nonstationary local mean is subtracted from each spectral pixel. The local mean μ_b is obtained by sliding a double concentric window (a small inner window region [IWR] centered within a larger outer window region [OWR]; see figure 1) over every spectral pixel in the image and calculating the mean of the spectral pixels falling within the outer window. The size of the inner window is assumed to be the size of the typical target of interest in the image. The residual signal after mean subtraction is assumed to approximate a zero-mean pixel-to-pixel independent Gaussian random process. Let each input spectral signal consisting of J spectral bands be denoted by $\mathbf{x}(n) = (x_1(n), x_2(n), \dots, x_J(n))^T$. Define \mathbf{X}_b to be a $J \times M$ matrix of M centered (mean-removed) reference background clutter pixels (or pixels in the outer window). Each observation spectral pixel is represented as a column in the sample matrix $\mathbf{X}_b = [\mathbf{x}(1), \mathbf{x}(2), \dots, \mathbf{x}(M)]$.

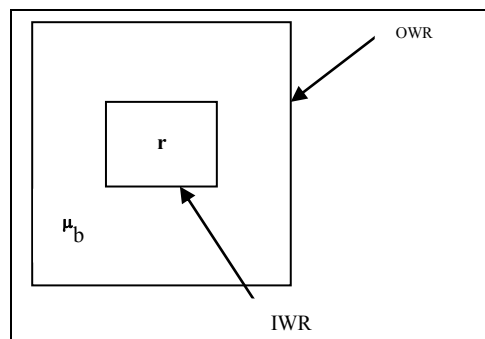


Figure 1. A sliding dual window: an IWR and an OWR.

Consider a test pixel \mathbf{r}_{ij} at pixel location ij . The RX algorithm output at each pixel is given by the following:

$$\delta_{\text{rx}}(\mathbf{r}_{ij}) = (\mathbf{r}_{ij} - \hat{\boldsymbol{\mu}}_b)^T \hat{\mathbf{C}}_b^{-1} (\mathbf{r}_{ij} - \hat{\boldsymbol{\mu}}_b), \quad (1)$$

where \mathbf{r}_{ij} represents the pixel under consideration located at the center of the IWR, $\hat{\boldsymbol{\mu}}_b$ represents the estimated mean of the pixels within the OWR, and $\hat{\mathbf{C}}$ is the estimated covariance matrix of the pixels within the OWR given by $\hat{\mathbf{C}} = (1/N) \mathbf{X}_b \mathbf{X}_b^T$.

The size of the dual window is set such that the IWR encloses a target-sized region and the OWR includes its surrounding region. If the dual window is placed within a spatially homogeneous region consisting of similar types of materials, such as natural backgrounds, the statistical characteristics of the IWR and OWR will be similar to each other. The IWR and OWR will contain significantly different statistical features if the dual window is centered on a region where the target is surrounded by the local background. Use of appropriate thresholding on the RX output (equation 1) allows most targets to be detected as anomalies.

The dual window RX algorithm (equation 1) is easily applied to each HS pixel since these pixels are already in vector form. However, in the case of high resolution SAR each co-registered HS pixel corresponds to a block of pixels in the SAR image due to the difference in spatial resolution between the SAR and HS. For SAR imagery we group all the pixels that physically correspond to a single HS pixel and represent them as a SAR vector pixel. This process is done for each corresponding HS pixel in order to form a SAR cube image of the same spatial resolution as HS image. It should be noted that the number of corresponding SAR pixels to each HS pixel will obviously be different from the number of spectral bands in HS. Now the RX-algorithm can be applied separately to the HS and SAR cubes of the same resolution to obtain the anomalies from each sensor data.

To develop an RX-like joint fusion and anomaly detection algorithm, let each pixel located at (i, j) in the HS image be represented by a vector $\mathbf{x}_h(i, j)$ consisting of J spectral bands and the corresponding block of pixels centered at (i, j) be represented by $\mathbf{x}_s(i, j)$ consisting of P pixels since for practical platforms, the SAR image has much higher resolution than the HS sensor. Furthermore, let the concatenated vectors from the two sensors corresponding to the same HS pixel location (i, j) after normalization be represented by a partition vector $\mathbf{x}_{\text{hs}}(i, j) =$

$$\begin{bmatrix} \mathbf{x}_h(i, j) \\ \mathbf{x}_s(i, j) \end{bmatrix}, \text{ where } \mathbf{x}_h(i, j) \text{ and } \mathbf{x}_s(i, j) \text{ are the pixels under consideration at the center of the dual}$$

window in the HS and SAR images, respectively. Applying the RX algorithm on the concatenated data $\mathbf{x}_{\text{hs}}(i, j)$ is given by the following:

$$\delta_{\text{rx}}^{\text{hs}}(i,j) = \left(\begin{bmatrix} \mathbf{x}_h(i,j) \\ \mathbf{x}_s(i,j) \end{bmatrix} - \begin{bmatrix} \hat{\boldsymbol{\mu}}_h \\ \hat{\boldsymbol{\mu}}_s \end{bmatrix} \right)^T \begin{pmatrix} \hat{\mathbf{C}}_{\text{hh}} & \hat{\mathbf{C}}_{\text{hs}} \\ \hat{\mathbf{C}}_{\text{sh}} & \hat{\mathbf{C}}_{\text{ss}} \end{pmatrix}^{-1} \left(\begin{bmatrix} \mathbf{x}_h(i,j) \\ \mathbf{x}_s(i,j) \end{bmatrix} - \begin{bmatrix} \hat{\boldsymbol{\mu}}_h \\ \hat{\boldsymbol{\mu}}_s \end{bmatrix} \right), \quad (2)$$

where $\hat{\boldsymbol{\mu}}_h$ and $\hat{\boldsymbol{\mu}}_s$ are the estimated means of all the pixels (\mathbf{x}_h and \mathbf{x}_s) in the corresponding outer windows and $\hat{\mathbf{C}}_{\text{hh}}$ and $\hat{\mathbf{C}}_{\text{ss}}$ are the estimated covariance matrices of the HS and SAR data, respectively. In equation 2, the linear correlation between the HS and SAR data is exploited through the inverse covariance matrix of the concatenated data. If the SAR data is not linearly correlated to the HS data $\hat{\mathbf{C}}_{\text{hs}} = \hat{\mathbf{C}}_{\text{sh}} = 0$ in equation 2, then the joint fusion/detection algorithm is the same as performing the RX on each sensor data separately and adding the results.

2.2 Nonlinear Joint Fusion and Detection Using SAR and HS at the Pixel Level

One way to exploit the higher-order correlation between the two data is to *explicitly* map each sensor data into a higher dimension by a nonlinear mapping. For example, assume the input hyperspectral data is represented by the data space ($\mathcal{X} \subseteq \mathbf{R}^d$) and \mathcal{F} is a feature space associated with \mathcal{X} by a nonlinear mapping function.

$$\begin{aligned} \Phi: \mathcal{X} &\rightarrow \mathcal{F} \\ \mathbf{x}_h(i,j) &\mapsto \Phi(\mathbf{x}_h(i,j)), \end{aligned} \quad (3)$$

where $\mathbf{x}_h(i,j)$ is an input vector which is mapped into a potentially much higher (possibly infinite) dimensional feature space. Any linear anomaly technique can now be remodeled into this high-dimensional feature space by replacing the original input data $\mathbf{x}_h(i,j)$ with the mapped data $\Phi(\mathbf{x}_h(i,j)) = \mathbf{x}_\phi^h(i,j)$. Due to the high dimensionality of the feature space, \mathcal{F} , it is computationally not feasible to directly implement any algorithm in this feature space. However, kernel-based learning techniques use an effective kernel trick given by the following:

$$k(\mathbf{x}, \mathbf{y}) = \langle \Phi(\mathbf{x}), \Phi(\mathbf{y}) \rangle = \Phi(\mathbf{x})^T \Phi(\mathbf{y}), \quad (4)$$

which implements a dot product between two vectors in the feature space by employing a kernel function k associated with the nonlinear mapping Φ . Using the kernel trick representation (equation 4), allows us to implicitly compute the dot products in \mathcal{F} without mapping the input vectors into \mathcal{F} . Therefore, in the kernel methods, the mapping function, Φ , does not have to be identified. A dot product in \mathcal{F} can be avoided and replaced by a kernel function, k , a nonlinear function which can be easily calculated without identifying the nonlinear map, Φ .

A preferred kernel to utilize is the Gaussian radial basis function kernel:

$$k(\mathbf{x}, \mathbf{y}) = \exp\left(\frac{-\|\mathbf{x} - \mathbf{y}\|^2}{\sigma}\right), \text{ where } \sigma > 0 \text{ is a constant.}$$

Kwon and Nasrabadi³ show how to extend the RX algorithm given by equations 1 or 2 to a nonlinear version (so-called kernel RX) by using the idea of kernel-based learning theory. The kernel version of the linear RX algorithm³ for HS and SAR sensor data is given by equations 5 and 6, respectively.

$$\delta_{\text{KRX}}^{\text{h}}(i, j) = (\mathbf{k}_{\mathbf{x}_h} - \mathbf{k}_{\boldsymbol{\mu}_h})^{\text{T}} \mathbf{K}_{\mathbf{x}_{\text{hh}}}^{-2} (\mathbf{k}_{\mathbf{x}_h} - \mathbf{k}_{\boldsymbol{\mu}_h}), \quad (5)$$

and

$$\delta_{\text{KRX}}^{\text{s}}(i, j) = (\mathbf{k}_{\mathbf{x}_s} - \mathbf{k}_{\boldsymbol{\mu}_s})^{\text{T}} \hat{\mathbf{K}}_{\mathbf{x}_{\text{ss}}}^{-2} (\mathbf{k}_{\mathbf{x}_s} - \mathbf{k}_{\boldsymbol{\mu}_s}), \quad (6)$$

where $\mathbf{k}_{\mathbf{x}_h} = k(\mathbf{X}_h, \mathbf{x}_h(i, j))$, $\mathbf{k}_{\mathbf{x}_s} = k(\mathbf{X}_s, \mathbf{x}_s(i, j))$, $\mathbf{k}_{\boldsymbol{\mu}_h} = k(\mathbf{X}_h, \boldsymbol{\mu}_h(i, j))$, and $\mathbf{k}_{\boldsymbol{\mu}_s} = k(\mathbf{X}_s, \boldsymbol{\mu}_s(i, j))$ are the kernel empirical expansion maps and similarly, $\mathbf{K}_{\mathbf{x}_{\text{hh}}} = \mathbf{K}(\mathbf{X}_h, \mathbf{X}_h) = (\mathbf{K})_{ij}$ and $\mathbf{K}_{\mathbf{x}_{\text{ss}}} = \mathbf{K}(\mathbf{X}_s, \mathbf{X}_s) = (\mathbf{K})_{ij}$ are $N \times N$ kernel (gram) matrices whose entries are the dot products $\langle \Phi(\mathbf{x}_h(i)), \Phi(\mathbf{x}_h(j)) \rangle$ and $\langle \Phi(\mathbf{x}_s(i)), \Phi(\mathbf{x}_s(j)) \rangle$, respectively. \mathbf{X}_h and \mathbf{X}_s are matrices whose columns represent the data in the outer window of HS and SAR, respectively. The kernel RX version for the concatenated data is given by the following:

$$\delta_{\text{KRX}}^{\text{hs}}(i, j) = (\mathbf{k}_{\mathbf{x}_{\text{hs}}} - \mathbf{k}_{\boldsymbol{\mu}_{\text{hs}}})^{\text{T}} \mathbf{K}_{\mathbf{x}_{\text{hs}}}^{-2} (\mathbf{k}_{\mathbf{x}_{\text{hs}}} - \mathbf{k}_{\boldsymbol{\mu}_{\text{hs}}}), \quad (7)$$

where $\mathbf{k}_{\mathbf{x}_{\text{hs}}} = \mathbf{k}_{\mathbf{x}_h} + \mathbf{k}_{\mathbf{x}_s}$, $\mathbf{k}_{\boldsymbol{\mu}_{\text{hs}}} = \mathbf{k}_{\boldsymbol{\mu}_h} + \mathbf{k}_{\boldsymbol{\mu}_s}$, and $\mathbf{K}_{\mathbf{x}_{\text{hs}}} = \mathbf{K}_{\mathbf{x}_{\text{hh}}} + \mathbf{K}_{\mathbf{x}_{\text{ss}}}$, which is a $N \times N$ kernel matrix whose entries are the dot products.

$$\begin{aligned} (\mathbf{K}_{\mathbf{x}_{\text{hs}}})_{ij} &= k(\mathbf{x}_{\text{hs}}(i), \mathbf{x}_{\text{hs}}(j)) = \langle \{\Phi(\mathbf{x}_h(i)), \Phi(\mathbf{x}_s(i))\}, \{\Phi(\mathbf{x}_h(j)), \Phi(\mathbf{x}_s(j))\} \rangle \\ &= \langle \{\Phi(\mathbf{x}_h(i)), \Phi(\mathbf{x}_h(j))\} \rangle + \langle \{\Phi(\mathbf{x}_s(i)), \Phi(\mathbf{x}_s(j))\} \rangle. \end{aligned} \quad (8)$$

Using different kernel functions or appropriately weighting the kernel functions for HS or SAR can achieve different fusion results.

3. Results

The hyperspectral mine image consists of 70 bands over the spectral range of 8–11.5 μm , which includes the long-wave infrared band. The SAR images used were produced from a SAR sensor operating in the high- and low-frequency range. Figure 2a and b shows the co-registered SAR and HS images, which contain surface mines and disturbed soil representing buried mines, respectively. The RX anomaly detector has been implemented, as well as the kernel RX, to detect mines in SAR and HS images separately and on concatenated SAR/HS data to obtain a

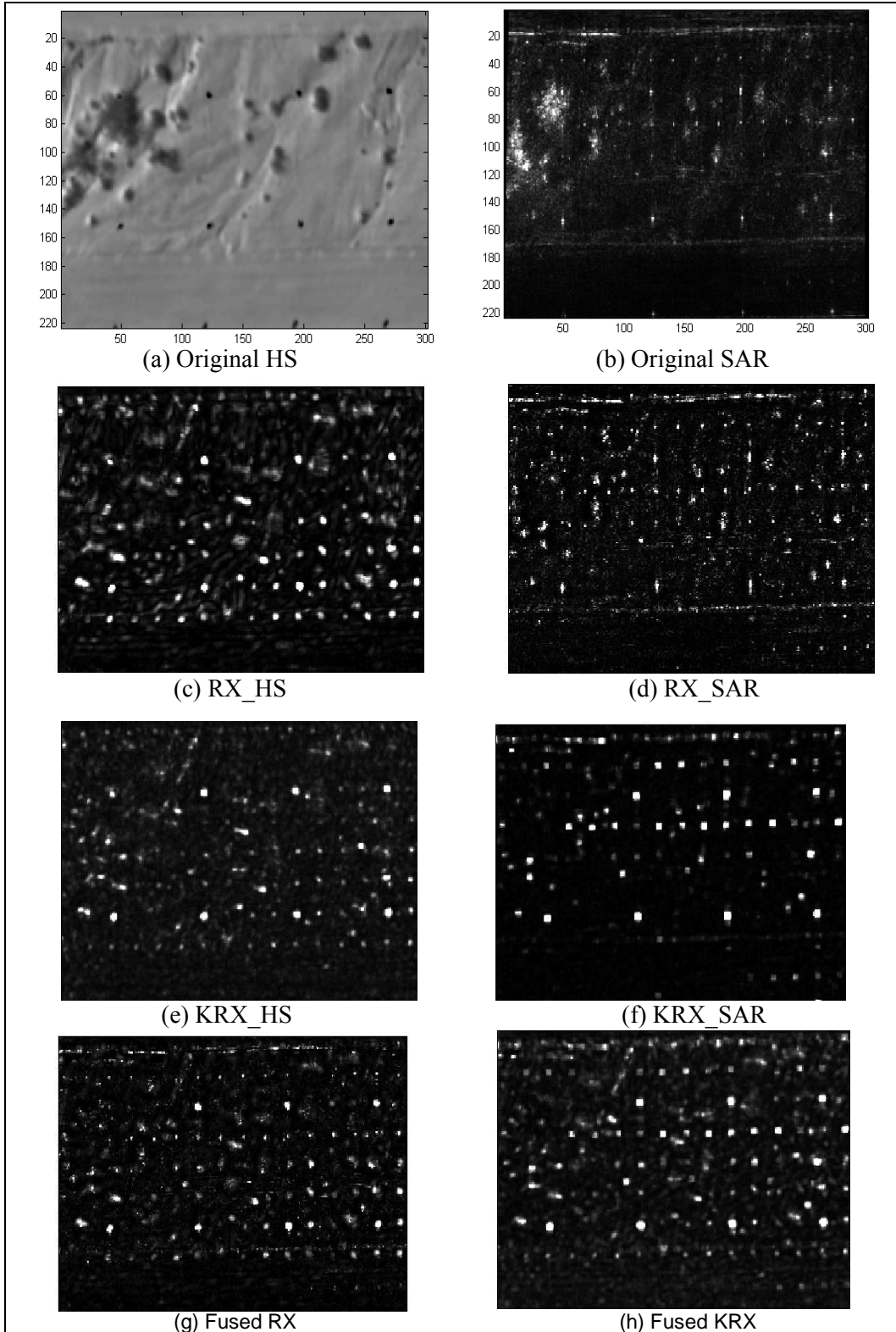


Figure 2. (a) HS image, (b) SAR image, (c) RX detected mines for HS, (d) RX detected mines for SAR, (e) kernel RX detected mines for HS, (f) kernel RX detected mines for SAR, (g) joint linear fusion/detection RX results, and (h) joint nonlinear fusion/detection KRX results.

joint fusion/detection algorithm. Figure 2a and b shows the original HS and SAR images of the same region that are processed, respectively. Results of the RX algorithm and kernel RX are shown in figure 2c–f. Figure 2g and h shows the joint linear and nonlinear fusion/detection results using the concatenated data, and the ROC curves are represented in figure 3. It is clear from figure 3 that the nonlinear joint fusion/detection algorithm performance exceeds the linear RX as well as the single sensor results.

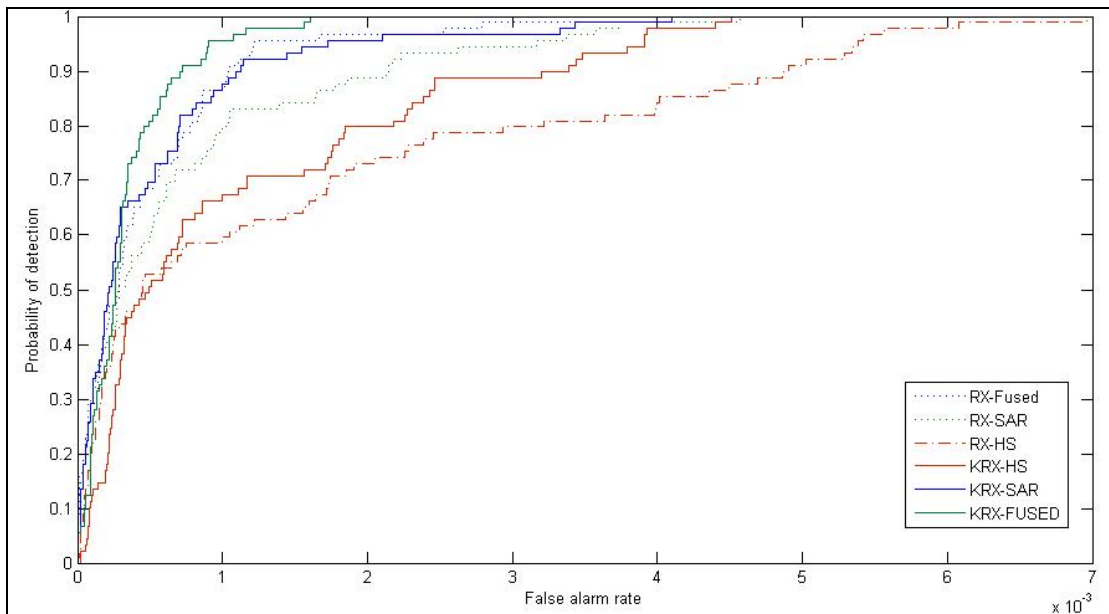


Figure 3. The ROC plots for the conventional RX and kernel RX algorithms.

4. Conclusions

A nonlinear fusion algorithm for detection of surface and buried mines has been designed. Nonlinear pixel level joint fusion and detection were developed based on the in-house kernel RX algorithm. The nonlinear correlation between the SAR and HS data was exploited in the pixel-based fusion and detection algorithm. Use of different kernels as well as developing procedures for weighting the kernels is still to be investigated.

NO. OF
COPIES ORGANIZATION

1 DEFENSE TECHNICAL
(PDF INFORMATION CTR
ONLY) DTIC OCA
8725 JOHN J KINGMAN RD
STE 0944
FORT BELVOIR VA 22060-6218

1 DIRECTOR
US ARMY RESEARCH LAB
IMNE ALC IMS
2800 POWDER MILL RD
ADELPHI MD 20783-1197

1 DIRECTOR
US ARMY RESEARCH LAB
AMSRD ARL CI OK TL
2800 POWDER MILL RD
ADELPHI MD 20783-1197

1 DIRECTOR
US ARMY RESEARCH LAB
AMSRD ARL CI OK T
2800 POWDER MILL RD
ADELPHI MD 20783-1197

1 DIRECTOR
US ARMY RESEARCH LAB
AMSRD ARL RO EV
W D BACH
PO BOX 12211
RESEARCH TRIANGLE PARK
NC 27709

ABERDEEN PROVING GROUND

1 DIR USARL
AMSRD ARL CI OK TP (BLDG 4600)

NO. OF COPIES ORGANIZATION

- 1 US ARMY CERDEC NVESD
AMSRD CER NV OD
J RATCHES
10221 BURBECK RD STE 430
FT BELVOIR VA 22060-5806
- 2 US ARMY CERDEC NVESD
AMSRD CER NV ST
J HILGER
P PERCONTI
10221 BURBECK RD STE 430
FT BELVOIR VA 22060-5806
- 1 US ARMY CERDEC NVESD
AMSRD CER NV MS
R DRIGGERS
10221 BURBECK RD STE 430
FT BELVOIR VA 22060-5806
- 1 US ARMY RDECOM AMRDEC
AMSRD AMR SG IP
H ANDERSON
BLDG 5400
REDSTONE ARSENAL AL 35898
- 1 US ARMY RDECOM AMRDEC
AMSRD AMR SG
W PITTMAN
BLDG 5400
REDSTONE ARSENAL AL 35898
- 1 US ARMY RDECOM AMRDEC
AMSRD AMR SG IR
R SIMS
BLDG 5400
REDSTONE ARSENAL AL 35898
- 1 US ARMY RDECOM AMRDEC
AMSRD AMR WS PL
W DAVENPORT
BLDG 7804
REDSTONE ARSENAL AL 35898
- 1 US ARMY AVN & MIS CMND
AMSAM RD
W C MCCORKLE
REDSTONE ARSENAL AL 35898-5240
- 1 US ARMY NATICK RDEC
ACTING TECHL DIR
SBCN TP T
P BRANDLER
KANSAS ST BLDG 79
NATICK MA 01760-5056

NO. OF COPIES ORGANIZATION

- 1 US ARMY TACOM
AMSRD TAR R
G R GERHART
MS 263
6501 E ELEVEN MILE RD
WARREN MI 48397-5000
- 1 COMMANDER
US ARMY TRADOC
SCIENCE & TECHLGY DIV
ATFC
J KINCAID
FT MONROE VA 23651-5850
- 1 US ARMY ARDEC
AMSTA AR A
BLDG 1
PICATINNY ARSENAL NJ 07806-5000
- 1 US ARMY RDECOM ARDEC
RADIOGRAPHIC LAB
AMSRD AAR AEP S
P WILLSON
BLDG 94
PICATINNY ARSENAL NJ 07806-5000
- 1 US ARMY RDECOM ARDEC
RADIOGRAPHIC LAB
AMSRD AAR AEP S
J ROMANO
BLDG 924
PICATINNY ARSENAL NJ 07806-5000
- 1 US ARMY TRADOC
BATTLE LAB INTEGRATION &
TECHL DIR
ATCH B
10 WHISTLER LANE
FT MONROE VA 23651-5850
- 1 COMMANDER USAISEC
AMSEL TD
BLAU
BLD 61801
FT HUACHUCA AZ 85613-5300
- 2 DARPA
J RICKLIN
S WELBY
3701 N FAIRFAX DR
ARLINGTON VA 22203-1714

NO. OF
COPIES ORGANIZATION

- 1 NGA
R S RAND
MS DN 11
12310 SURSISE VALLEY DR
RESTON VA 20191-3449
- 1 AFRL/SNAA
M JARRATT
AREA B BLDG 620
2241 AVIONICS CIR
WPAFB OH 45433-7321
- 1 CMTCO
A SUZUKI
1030 S HIGHWAY A1A
PATRICK AFB FL 23925-3002
- 3 SITAC
H STILES
K WHITE
R DOWNIE
STE 500
11981 LEE JACKSON
MEMORIAL HWY
FAIRFAX VA 22033-3309
- 1 US MILITARY ACADEMY
MATHEMATICAL SCIENCE CTR
OF EXCELLENCE
PHOTONICS CENTER
THAYER HALL RM 226C
J HARTKE
WEST POINT NY 10996-1786
- 1 DIRECTOR
US ARMY RESEARCH LAB
AMSRD ARL RO MI
L DAI
BLDG 4300
PO BOX 12211
RSRCH TRIANGLE PARK NC 27703
- 1 DIRECTOR
US ARMY RESEARCH LAB
AMSRD ARL RO MM
D ARNEY
BLDG 4300
PO BOX 12211
RSRCH TRIANGLE PARK NC 27703

NO. OF
COPIES ORGANIZATION

- 1 DIRECTOR
US ARMY RESEARCH LAB
AMSRD ARL RO M
R ZACHERY
BLDG 4300 RM 249
PO BOX 12211
RSRCH TRIANGLE PARK NC 27703
- 1 DIRECTOR
US ARMY RESEARCH LAB
AMSRD ARL RO MM
H CHANG
BLDG 4300 RM 249
PO BOX 12211
RSRCH TRIANGLE PARK NC 27703
- 1 DIRECTOR
US ARMY RESEARCH LAB
AMSRD ARL SE
J PELLEGRINO
BLDG 207 RM 4D-28
2800 POWDER MILL RD
ADELPHI MD 20783-1197
- 1 DIRECTOR
US ARMY RESEARCH LAB
AMSRD ARL SE
N SROUR
BLDG 202 RM 3G124
2800 POWDER MILL RD
ADELPHI MD 20783-1197
- 1 DIRECTOR
US ARMY RESEARCH LAB
AMSRD ARL SE S
J EICKE
BLDG 202 RM 3G020
2800 POWDER MILL RD
ADELPHI MD 20783-1197
- 1 DIRECTOR
US ARMY RESEARCH LAB
AMSRD ARL SE SE
N NASRABADI
BLDG 204 RM 2C118
2800 POWDER MILL RD
ADELPHI MD 20783-1197

NO. OF
COPIES ORGANIZATION

1 DIRECTOR
US ARMY RESEARCH LAB
AMSRD ARL SE SE
L KAPLAN
BLDG 202 RM 3F082
2800 POWDER MILL RD
ADELPHI MD 20783-1197

1 DIRECTOR
US ARMY RESEARCH LAB
AMSRD ARL SE SE
A CHAN
BLDG 202 RM 3F068
2800 POWDER MILL RD
ADELPHI MD 20783-1197

ABERDEEN PROVING GROUND

1 DIRECTOR
USAMSAA
AMSRD AMS SC
J MAZZ
BLDG 328 RM 155
392 HOPKINS RD
APG MD 21005-5071

1 DIRECTOR
USAMSAA
AMSRD AMS SC
G KISTNER
BLDG 392 RM 201A
392 HOPKINS RD
APG MD 21005-5071

1 DIRECTOR
USAMSAA
AMSRD AMS SC
R WHEELER
392 HOPKINS RD
APG MD 21005-5071

1 US ARMY SOLDIER &
BIOLOGICAL CHEMICAL CMND
EDGEWOOD CHEMICAL &
BIOLOGICAL CTR
AMSSB RRT DP
W LOEROP
BLDG E 5554
APG MD 21020-5424

NO. OF
COPIES ORGANIZATION

1 US ARMY ATC
CSTE DTC AT TC N
D JENNINGS
400 COLLERAN RD
APG MD 21005-5059

1 US ARMY ATC
CSTE DT AT WC A
F CARLEN
BLDG 355
400 COLLERAN RD
APG MD 21005-5009

2 DIR USARL
AMSRD ARL WM BF
W OBERLE
AMSRD ARL VT UV
G HAAS

INTENTIONALLY LEFT BLANK.